Analytical model for the sound pressure waveform radiated underwater when an offshore steel pipe pile is driven with an impact hammer

Marshall V HALL[1]

[1] Marshall Hall Acoustics, Australia

ABSTRACT

An analytical model has been developed for the pressure waveform radiated underwater when an offshore steel pipe pile is struck by a hammer. The model is based on the coupled equations of motion for axial and radial vibration of a thin shell and yields frequency-dependent phase velocity and attenuation of these vibrations. A harmonic solution is obtained for the radiated sound pressure, using Junger and Feit's "Transform formulation of the pressure field of cylindrical radiators", which uses a Fourier Transform over vertical wavenumber. The model is applied to a comprehensively described measurement of a 6-tonne hammer driving a pile 32 m long and 76-cm in diameter. The pressure waveforms at horizontal range 12 m are examined at two mid-water hydrophone depths. The correlations between the model waveforms and the measured waveforms are high. For the main positive and negative peaks, the present model yields an average Peak-SPL of 219 dB re 1 µPa, which is 2 dB higher than the average of the corresponding measurements. Possible causes of this small difference are discussed.

Keywords: Underwater Noise I-INCE Classification of Subjects Number: 54.3

1. INTRODUCTION

Offshore impact pile-driving radiates regular pulses of loud noise underwater, and a substantial amount of data has been presented in the literature on the measured peak pressure of these pulses. For piles made of steel, the peak pressure at a horizontal range of around 10 m is usually in the region of 1 atmosphere (100 kPa). The quantity of descriptive measured data on noise from offshore pile driving is large. There have been several papers that use a Finite Element Method (FEM) to model the physics of the impact and the consequent wall vibration, and the results have been numerical rather than analytical. There have been many papers that used finite-element methods to model axial displacement for the purpose of predicting pile-driver performance (beginning with [1]), but these papers modelled the pile as a solid rod and also neglected radial vibration. It is generally accepted that the major underwater signals originate from radial vibration of the submerged portion of a pile, and there have been few papers that present an analytical model for radial vibration based on analytical solutions of the equations of motion.

Following an axial impact on a steel pile, a pulse of radial vibration (a bulge) travels down the pile much faster than sound travels through water. The first arrival at a hydrophone, described as a Mach wave, therefore originates from a point on the pile a little shallower than the hydrophone. The trailing signal will be due to multipaths from portions of the pile both above and below the originating point. A significant paper [2] reported the use of FEM for the vibration generated by an impact hammer, and described the important contribution of the Mach wave.

The objective of the present paper is to present results from an analytical model for the vibration of a cylindrical shell and the consequent peak pressure of sound radiation. A harmonic solution is obtained for the radiated sound pressure, using Junger and Feit's "Transform formulation of the pressure field of cylindrical radiators" [3]. The value of such a model is that it allows the relative importance of the driving parameters to be readily estimated and, in appropriate scenarios, can serve as a benchmark for FEM.

[1] marshallhall@optushome.com.au

2. DEVELOPMENTS IN THE SHELL VIBRATION MODEL

The model produces an analytical expression for the spectrum of the vibration of a finite pipe pile when struck axially by a short hammer. It is assumed that no hammer cushion is present. The coupled equations of motion for azimuth-independent axial and radial vibration (u and w) of a thin shell are solved. "For the thin-walled assumption to be valid the vessel must have a wall thickness of no more than about one-tenth (often cited as one twentieth) of its radius. This allows for treating the wall as a surface" [4]. The model yields frequency-dependent phase velocity and attenuation (due to radiation) for axial and radial vibration, and produces a complete description of the shell vibration. The present model is an extension of the previous model [5], in that a pile of finite length and the consequent reflections are now treated. The present model builds on Equations (1) to (34) therein, albeit with the following amendments and qualifications:

2.1 Initial velocity of the pile face

In a hammer without a cushion, there is an anvil (impact block) and a helmet (drive cap) between the ram and the pile. The ram, anvil and helmet are assumed to be incompressible, and to remain in contact after impact with a common velocity (v_c) that is obtained from conservation of momentum:

$$v_c = v_{ram} M_{ram} / \left(M_{ram} + M_{anvil} + M_{helmet} \right)$$

where v_{ram} is the velocity of the ram just prior to impact. For the impact between the helmet and the elastic pile face, it is assumed they have a common initial velocity (v_0) following impact which is (also) obtained from conservation of momentum (assuming the helmet and pile have the same longitudinal sound speeds):

$$v_0 / v_c = A_{helmet} / \left(A_{helmet} + A_{pile} \right)$$

where A_{helmet} and A_{pile} are the cross-sectional areas of the helmet and pile respectively.

2.2 Boundary condition at the pile face

In deriving a boundary condition on the axial displacement (u) at the pile face in [5] it was assumed that the phase velocity of u would equal q_h and thus be frequency-independent. As will be discussed later, the phase velocity (V) varies with frequency, and in particular $V \rightarrow q_y$ as $f \rightarrow 0$ if the internal medium is a gas or vacuum, whereas $V \rightarrow q_h$ as $f \rightarrow \infty$ for any medium, where

$$q_y = \sqrt{Y / \rho_s} \ , \ q_h = q_y \Big/ \sqrt{1 - \nu^2}$$

in which Y, ρ_s and ν are the Young modulus, density and Poisson ratio of the pile (steel) material. The assumption of a constant V is therefore an approximation, and further work will be required to obtain a more accurate model.

2.3 Boundary condition at the pile wall

In deriving an expression for the Specific Acoustic Impedance (SAI) at the pile wall in [5] it was assumed that the medium inside the pile was a vacuum. It is now assumed that the internal medium is the same as the external medium, and the SAI at the wall as previously expressed is now identified as the external SAI. These external and internal SAI are given by:

$$Z_n^{ext}(\omega) = i \omega \rho_n H_0^{(2)}(\xi a) / \xi H_1^{(2)}(\xi a)$$

$$Z_n^{\text{int}}(\omega) = i \omega \rho_n J_0[\xi(a-h)] / \xi J_1[\xi(a-h)]$$

where:
a is the external pile radius,
n denotes the medium (1 for air, 2 for water, 3 for seabed), and

$$\xi = \omega \sqrt{1/c_n^2 - 1/V_n(\omega)^2}$$

The "net" SAI that plays a role in the subsequent analysis is the difference between them.

2.4 Radial vibration

A shallow water environment is considered. The Fourier Transform of the pile wall's radial displacement w_n (z,t) in medium n will be denoted by $W_n(z,\omega)$. The water layer (0 < z < D, where D is the seafloor depth) will be referred to as medium 2. If reflections from the pile toe were neglected then $W_2(z,\omega)$ would be given by [5]:

$$W_2(z,\omega)=\frac{\nu v_0 q_h \exp(i\phi)}{a S_2(q_y,\omega) S_2(q_h,\omega)(\Omega+i\omega)}$$

where

$$\phi = -\omega H/V_1 - \omega z/V_2$$

$$S_n(q,\omega)=\sqrt{q^2/a^2-\omega^2+i\omega\left(Z_n^{ext}-Z_n^{\text{int}}\right)/\rho_s h}$$

$$\Omega = A_{pile} Y/M\, q_h$$

$$V_n(\omega)= q_h\, S_n(q_y,\omega)/S_n(q_h,\omega)$$

in which:

H is the height of the pile face (H > 0), and

M is the total mass of the hammer's ram, anvil and helmet.

If L denotes the length of the pile, then for positions on the pile below the seafloor (D < z < L - H), the expression for W_3 would be similar to that for W_2, except that ϕ would become

$$\phi = -\omega H/V_1 - \omega\, D/V_2 - \omega(z-D)/V_3$$

Because V is a function of S which in turn is a function of Z and hence V, V has to be obtained by iteration.

The above expression for W_2 corresponds to a downward travelling wave, which will be reflected upwards by the pile toe at depth L – H. The reflectivity will be less than unity, since some vibration will radiate from the toe into the seabed. The reflection will create an additional term in W_2, in which the parameter ϕ will be

$$\phi = +\omega(D-L-H)/V_3 + \omega(z-D)/V_2$$

The upward reflection will travel to the pile face (z = - H) where it will be reflected back downward. This cyclical behaviour will recur, but with diminishing amplitude.

3. SCENARIO

The model is applied here to the driving of a steel pile by an impact hammer without a cushion, as reported by [2]. The pile driving project occurred on Vashon Island in Washington State USA, during November 2009.

3.1 The pile and its environment

The dimensions of the pile were [2]: external radius 0.381 m, wall thickness 2.54 cm (radius /15), and length 31.9 m. Apart from noting that Poisson's ratio for steel is approximately 0.3, [2] did not give values for the other elastic properties of the pile steel. It will be assumed here that the steel density was the standard value of 7800 kg/m^3 [6]. According to [2], their FEM results indicated a longitudinal wave speed of 5015 m/s where surrounded by water, and 5082 m/s where surrounded by sediment. It would therefore be reasonable to assume that the longitudinal wave speed (q_y) used in their model was approximately 5000 m/s. This corresponds to a Young Modulus of 195 GPa, which is the minimum of the interval reported by [7]. It will be assumed here that the longitudinal loss factor (1/Q) is 3×10^{-4}, the maximum of the interval reported by [6]. This loss factor, which corresponds to an absorption rate of 0.008 dB per wavelength, is not a significant feature of the model.

The seafloor depth was 12.5 m and the pile was driven approximately 14 m into the seabed at the time of the measurements (the pile face was therefore at a height of 5.4 m). The seawater sound-speed (c_2) and the sediment sound-speed (c_3) were 1485 and 1625 m/s respectively [2], and the sediment density (ρ_3) was assumed to be 1.85 times the water density (ρ_2).

3.2 The hammer

The pile was driven with a Delmag diesel hammer model D62-22. According to the hammer manufacturer [8], the role of the diesel fuel is as follows:

> .. Injection of diesel fuel and compression. While dropping…a certain quantity of fuel is sprayed on top of the impact block. After passing the exhaust ports, the piston starts compressing the air in the combustion chamber. Impact and Combustion. The impact of the piston on the impact block atomizes the diesel fuel in the combustion chamber. The atomized fuel ignites in the highly compressed air. The combustion energy moves the piston upwards… Three different energies are acting on the pile: Compression + Impact + Combustion.

On a schematic diagram of Force vs time [9], the force on the pile due to compression is not shown (so presumed to be small), the force due to impact has a sharp peak, and the force due to combustion has a broad peak with an amplitude that is around one-half of the impact peak. On this basis, it will be assumed here that the effect of combustion on radiated peak sound pressure is negligible.

According to [2], the ram had a mass of 6200 kg and an impact velocity of 7.6 m/s. The masses of the anvil and helmet were 1285 and 2060 kg respectively [10].

4. RESULTS FROM THE SHELL VIBRATION MODEL

4.1 Spectra of phase velocity and damping rate

The longitudinal phase velocity, Real (V), is shown in Figure 1 as a function of frequency up to 10 kHz. In medium 1 (air), $V_1 \rightarrow q_y$ as $f \rightarrow 0$. In the denser liquid media, this limit is somewhat higher. As f becomes large, $V_n \rightarrow q_h$ for all three media. The large swings at frequency near 2.1 kHz are associated with the expression for S, in which it can be seen that V will be large at $\omega = q_y/a$ and q_h/a unless the SAI are also large (as will occur in a liquid). For the case studied, the two corresponding "critical" frequencies are 2089 and 2183 Hz. In medium 2, sharp minima and maxima occur at a regular spacing of 2.1 kHz at the higher frequencies. If there is no liquid in the pile interior, it was shown in [5] that V_2 increased rapidly from below q_y to above q_h as frequency increased past the critical frequencies, and then decreased monotonically to q_h as frequency continued to increase. The sharp regularly-spaced extrema may therefore be attributed to the liquid internal medium, and in particular to resonances in the standing waves therein. It can be seen that V_2 and V_3 have the values reported for them in [2] (5015 and 5082 m/s) at a frequency of approximately 1 kHz, which was the mid-point of their frequency band.

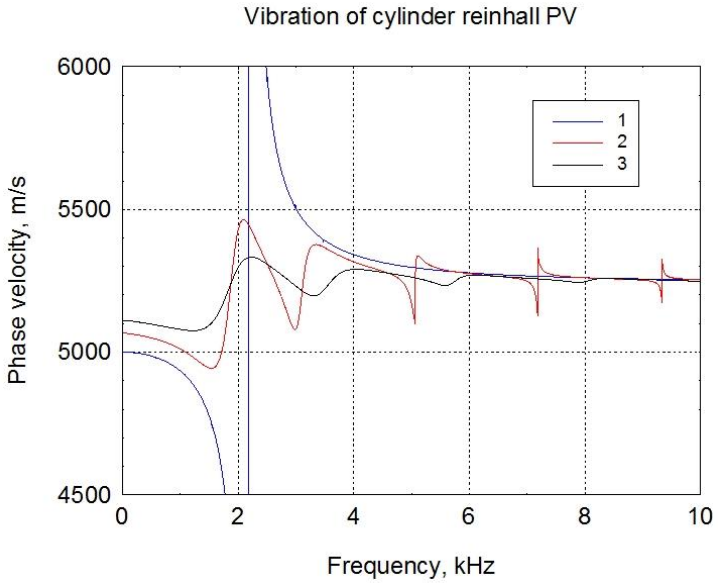

Figure 1: Longitudinal phase velocity vs frequency along the steel pile studied by [2] when surrounded by air (1), seawater (2) and sediment (3) respectively. Pile dimensions are radius 38 cm, wall thickness 2.5 cm.

The longitudinal damping rate (DR) in decibels per wavelength is shown as a function of frequency in Figure 2. At a given frequency f, the wavelength is obtained from $\lambda = V/f$, and this λ is multiplied by the damping in dB per unit length [proportional to Imag (V)] to yield damping per wavelength. In air (medium 1), this DR equals the intrinsic damping in steel, except near and between the two critical frequencies. In the liquid media the SAI are large, and no particular behavior occurs near the critical frequencies. The extrema spaced 2.1 kHz apart at the higher frequencies are again evident.

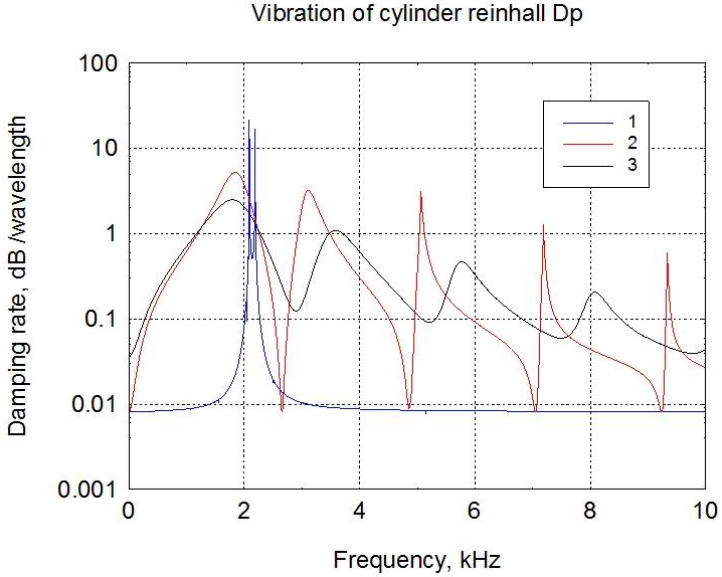

Figure 2: Longitudinal damping along the same pile whose phase velocity is presented in Figure 1.

4.2 Axial and radial vibrations of the pile wall

The Fourier Transforms (spectra) of the pile wall's axial and radial velocities at the pile face (z = -5.4 m) and at the water surface (z = 0) are shown in Figure 3. At the pile face the axial spectrum falls off monotonically with frequency, while at the water surface it has a deep minimum in the band between the two critical frequencies (due to the high damping in the band). At frequencies outside the critical band, the two axial spectra are indistinguishable (due to the negligible damping). The radial spectrum at the face has sharp peaks at the two critical frequencies, which transform into a deep minimum in the band between the critical frequencies.

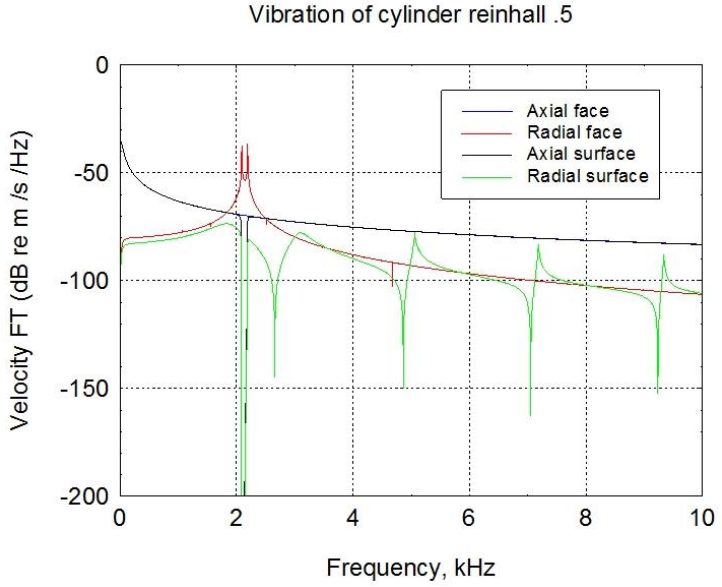

Figure 3: Fourier Transforms of the pile wall's axial and radial velocities at the pile face and water surface.

The waveforms of the pile wall's axial and radial velocities at the pile face are shown in Figure 4, and those at the water surface are shown in Figure 5. These (complex) inverse FTs were computed with a frequency pixel of 1.22 Hz (the integration time was specified to be 0.5 s, but the program increased this to 0.8 s in order to make the number of pixels an integer power of 2, and thus optimize the performance of the inverse FT algorithm). For negative frequencies the FT was set to the conjugate of its value at the "mirror" positive frequency, and thus the resulting waveform should be real. With this frequency pixel, the energy in the real part of the waveform was only 0.01 dB less than the energy in the spectrum (the shortfall increased if the frequency pixel was increased), and on this basis the real waveform is regarded as accurate. At the face, the axial velocity decays exponentially, while the radial velocity shows the beat behaviour that results from the peaks at the two critical frequencies. At the water surface, the axial velocity is approximately the same as at the face (apart from a 1-ms time delay), while the radial velocity has reduced markedly, due to the loss of the energy in the band between the critical frequencies. The reason for the decrease in radial velocity from the face to the surface is that the aerial portion of the pile has radiated sound into the air.

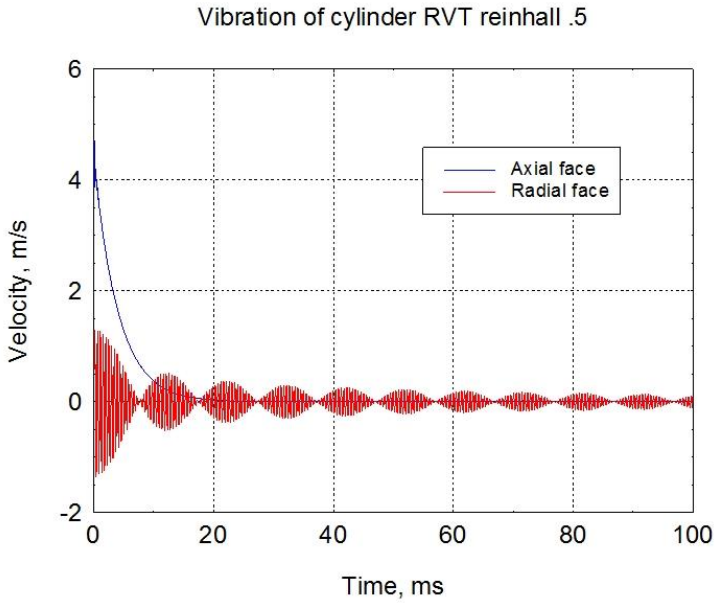

Figure 4: Waveforms of the pile wall's axial and radial velocities at the pile face.

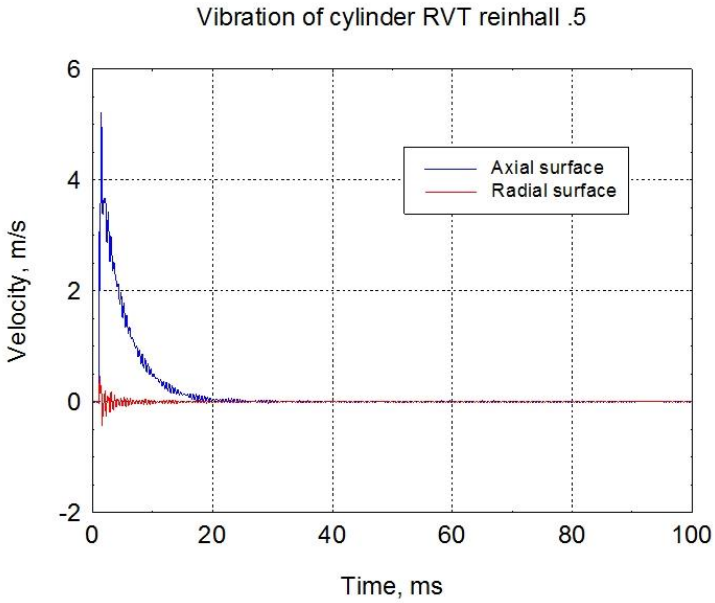

Figure 5: Waveforms of the pile wall's axial and radial velocities at the water surface.

5. RADIATED SOUND

5.1 Transform formulation of the pressure field of cylindrical radiators

The "Transform formulation of the pressure field of cylindrical radiators" [3] is applied to W(z,ω). The present model extends from the algorithm as implemented in [5] in two respects:

(i) Whereas [3] and [5] considered the surrounding medium to be unbounded, the present model modifies the algorithm to account for a free surface (at z = 0). The present model also assumes that a sound source above that surface will have no effect on a hydrophone below the surface.

(ii) Whereas [3] and [5] considered the surrounding medium to be homogeneous, the present model allows the value of V and DR on the pile to vary with depth in accordance with the properties of the surrounding medium. However, for a hydrophone within a particular medium, the model neglects the effect of the interface between media on propagation from the pile to the hydrophone. Radiation from the portion of the pile below the seafloor is included for a hydrophone in the water, but refraction at the seafloor is neglected.

5.2 Wavenumber (γ) Fourier Transform

The analysis in [3] used the vertical wavenumber (γ) Fourier Transform of the depth-dependence of radial vibration: F(γ) = FT{W(r,z,ω)}. F is a function of r and ω as well as γ, but these dependencies are suppressed for clarity. The frequency Fourier Transform of the pressure waveform p(r,z,t) will be denoted by P(r,z,ω), in which z is now hydrophone depth. The expression for P(r,z,ω) includes an inverse wavenumber-Fourier Transform of a function that contains F(γ) as a factor:

$$P(r,z,\omega) = \frac{\rho\omega^2 W(0,\omega)}{2\pi}\int_{-\infty}^{\infty}\frac{H_0^{(2)}(\xi r)\,F(\gamma)\exp(-i\gamma z)}{\xi H_1^{(2)}(\xi a)}d\gamma$$

$$\xi = \sqrt{k^2-\gamma^2}$$

For a surface reflectivity of -1 and no toe reflection, the wavenumber FT would be given by:

$$F(\gamma) = \int_0^{\infty}\exp\left[\frac{-i\omega z}{V_2(\omega)}\right]\exp[+i\gamma z]dz - \int_{-\infty}^{0}\exp\left[\frac{i\omega z}{V_2(\omega)}\right]\exp[+i\gamma z]dz$$

$$= \frac{i}{\gamma-\omega/V_2(\omega)} + \frac{i}{\gamma+\omega/V_2(\omega)}$$

When toe reflection is included, the expression for F(γ) is an infinite sum of down-going and up-going terms. An example of the resulting integrand in the expression for P(r,z,ω), computed for the [2] scenario, is shown in Figure 6. The parameters used for this display are: frequency 1 kHz, horizontal range 12 m, hydrophone depth 7.7 m (one of two hydrophone depths examined in detail in [2]), toe reflectivity -0.5, and pile-face reflectivity -1. The quasi-singularities near the ends occur at γ = ± k, where ξ = 0 and the Hankel function H_0 is singular. The peaks near γ = ± 1.2 and ±1.4 m^{-1} correspond to γ = ± ω /V_2(ω). The spread in the peaks is attributed to the dispersion in V_2, as displayed in Figure 1. At these peaks, the ratio γ /k ≈ 0.3.

At each frequency selected for the Inverse (frequency) Fourier Transform, which will be required in order to obtain p(r,z,t) from P(r,z,ω), the inverse γ-FT needs to be computed by numerical integration. The method chosen here is the straightforward (but slow) IMSL routine "QDAGS", which is an adaptive, general purpose routine for which endpoint singularities are acceptable. At each frequency, the integration intervals were defined as [- 1.2 ω/c_2, + 1.2 ω/c_2]. The stationary phase approximate method has been tried [11], but found to give large errors. These errors occur because for q > c, the peaks in F(γ) shown in Figure 6 are not points of stationary phase. The point of stationary phase is that γ for which γ /k = z /R, where R is the slant range. For z = 7.7 m, R = 14.26 m and γ /k is thus 0.54.

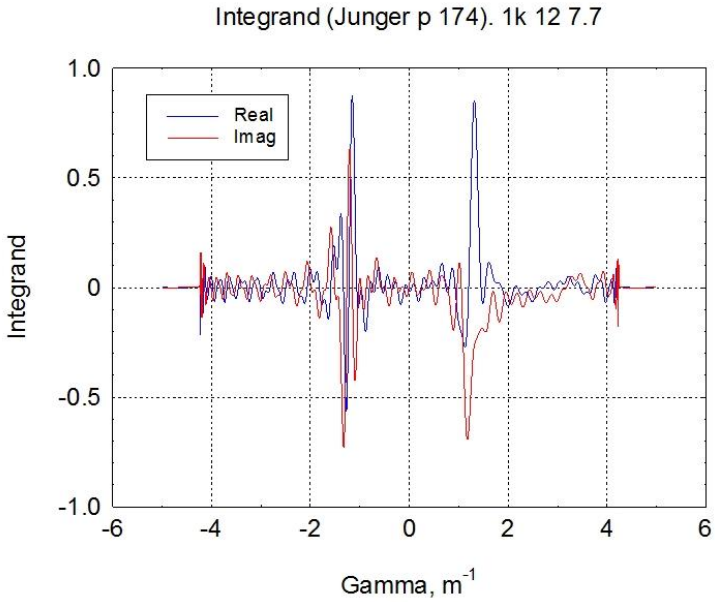

Figure 6: The gamma-dependent integrand in the expression for P(r,z,ω) for the [2] scenario. Frequency 1 kHz, horizontal range 12 m and hydrophone depth 7.7 m.

5.3 Sound pressure spectrum

Sound pressure spectra P(r,z,ω) have been computed for a horizontal range of 12 m and hydrophone depths of 7.7 and 10.5 m, the two depths examined in detail by [2]. The magnitudes of the results are shown in Figure 7. At frequencies below 1 kHz it can be seen that the spectral peaks at one depth are interleaved between those at the other. The values of the "frequency-SEL" obtained from the frequency integral $\int |P(\omega)|^2 \, df$ at the two depths are 185.77 and 184.16 dB re 1 $\mu Pa^2.s$ respectively.

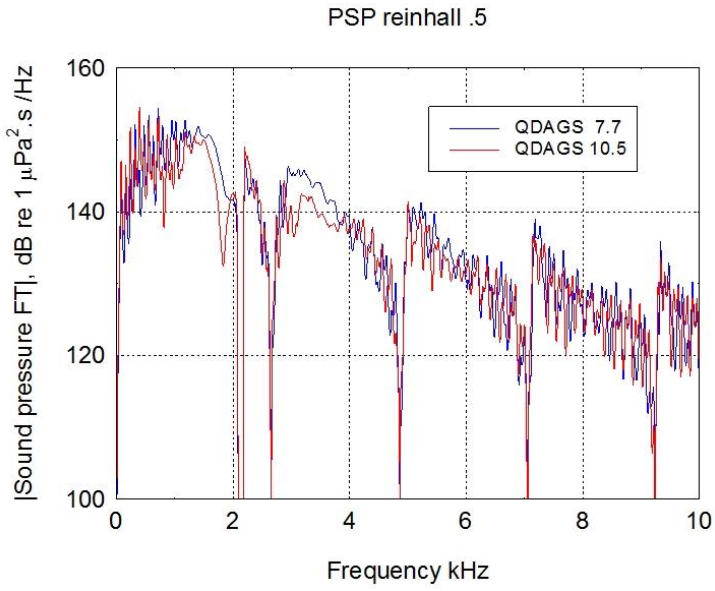

Figure 7: Fourier Transform of the radiated pressure at horizontal range of 12 m and hydrophone depths of 7.7 and 10.5 m, for the [2] scenario.

5.4 Sound pressure waveform

Sound pressure waveforms p(r,z,t) have also been computed for a horizontal range of 12 m and hydrophone depths of 7.7 and 10.5 m. The results are shown in Figure 8 over the time interval from 9 to 25 ms following impact. Each curve is the real part of a complex waveform produced by an inverse FFT with a frequency pixel of 1.22 Hz. The values of the "time-SEL" obtained from the time integral

$\int p(t)^2 dt$ at the two depths are 185.76 and 184.14 dB re 1 µPa^2.s respectively. Since these are only 0.01 and 0.02 dB less than the respective frequency-SELs, the frequency pixel used is regarded as sufficiently small to produce an accurate waveform.

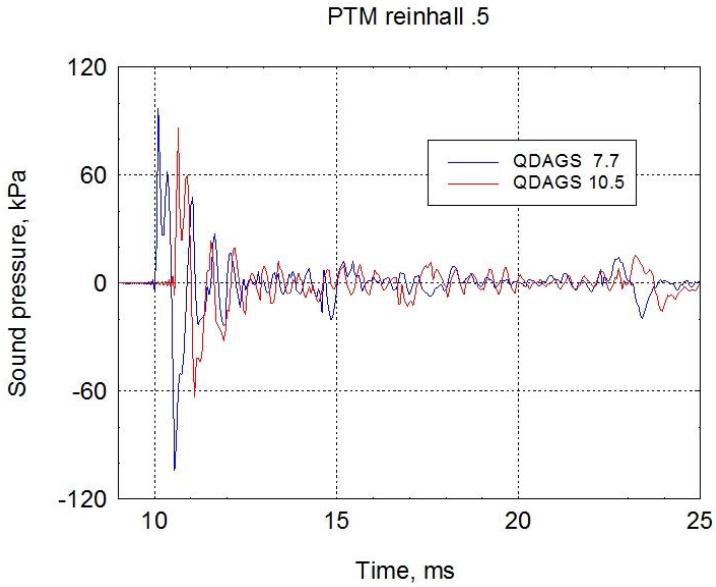

Figure 8: Radiated pressure waveforms over the time interval from 9 to 25 ms after impact, at horizontal range 12 m and hydrophone depths of 7.7 and 10.5 m, for the scenario in [2].

It is considered that each waveform is as accurate as can be obtained by this method in practice, in that with the frequency pixel of 1.22 Hz, the imaginary part has been observed to never exceed 4% of the real part. Since P(r,z,-ω) was set to P*(r,z,ω), the imaginary part would approach zero if the frequency pixel were further decreased, but the computer run-time would increase correspondingly. In addition, the error in the energy of the complete signal (the ratio of the frequency-SEL to the time-SEL) did not exceed 0.02 dB, as noted above. When a larger frequency pixel was used (in order to decrease computer run-time), it was observed that Imag{p(t)} increased, Real{p(t)} decreased, and time-SEL also decreased.

The pulses at around 17 to 18 ms in Figure 8 are Mach waves from the upward-travelling reflection from the pile toe; this reflection arrives at the deeper hydrophone before the shallower hydrophone. The pulses at around 23 ms are Mach waves from the subsequent downward travelling reflection from the pile face.

5.5 Comparison with data

On comparing each waveform in Figure 8 with the corresponding waveform in [2], it can be seen that they are highly correlated. The main difference is in the amplitudes of the initial positive and negative peaks. At 7.7-m depth the present model gives peaks of 97 and -104 kPa, which are 1.9 and 2.3 dB higher than the corresponding peaks in [2] (78 and -80 kPa). At 10.5-m depth the present model's peaks are 86 and -63 kPa, which are 0.8 and 0.4 dB higher than the corresponding peaks in [2] (78 and -60 kPa). In summary, for the average of the magnitudes of the four peaks (two positive and two negative), the present model yields 88 kPa (219 dB re 1 µPa), whereas the measurements yielded 74 kPa (217 dB re 1 µPa).

6. CONCLUSIONS

When applied to the conditions that prevailed during a comprehensively described measurement of pile noise, the present model yields radiated peak pressures that on average are 2 dB higher than were measured. One possible cause for this over-estimate could be the use of thin shell theory for the pile, for which the ratio of wall-thickness to radius was 1 /15. Another possible cause could be that, in deriving the relation between strain and particle velocity at the pile face, it was assumed (incorrectly) that phase velocity is independent of frequency.

REFERENCES

1. Smith EAL. Pile driving analysis by the wave equation. J Soil Mech and Found ASCE. 1960; 86: 35-61.
2. Reinhall PG, Dahl PH. Underwater Mach wave radiation from impact pile driving: Theory and observation, J Acoust Soc Am. 2011; 130 (3): 1209 – 1216.
3. Junger MC, Feit D. Sound, Structures, and Their Interaction. New York: Acoustical Society of America; 1993.
4. Anonymous. Cylinder Stress. Wikipedia http://en.wikipedia.org/wiki/Cylinder_stress. Retrieved 2014 Jul 16.
5. Hall MV. A semi-analytical model for non-Mach peak pressure of underwater acoustic pulses from offshore pile driving. Acoustics Australia. 2013; 41 (1): 42-51.
6. Irvine T. Damping properties of materials Revision C. 2004. http://syont.files.wordpress.com/2007/05/damping-properties-of-materials.pdf. Retrieved 2014 Jul 16.
7. Yarwood TM, Castle F. Physical and mathematical tables. London: Macmillan & Co. Ltd; 1959.
8. Anonymous. DELMAG Pile Driving Equipment Technical data. Esslingen Germany: DELMAG GmbH + Co.KG; 2010. http://www.delmag.com/technical-data.html Retrieved 2014 Jul 22.
9. Anonymous. DELMAG Pile driving equipment. Esslingen Germany: DELMAG GmbH + Co.KG; 2010. Downloaded from "DELMAG diesel pile hammers" www.delmag.com/diesel-pile-hammers.html Retrieved 2014 Aug 6
10. Anonymous. Delmag Diesel Hammers. Hazelwood, Missouri, USA: Hammer & Steel Inc. http://www.hammersteel.com/delmag-diesel-hammers.html. Retrieved 2014 Jul 19.
11. Hall MV. Development of a semi-analytical model for the underwater radiated noise from a driven pile – comparison of the stationary phase approximation with exact integration for computing an inverse Fourier Transform of vertical wavenumber (A). J Acoust Soc Am. 2014; 135 (4): 2300.